J Mater Sci (2006) 41:4823–4831
DOI 10.1007/s10853-006-0028-5

Spatially resolved self-sensing of strain and damage in carbon fiber cement

Sihai Wen · D. D. L. Chung

Received: 16 March 2005 / Accepted: 29 September 2005 / Published online: 2 May 2006

Abstract Spatially resolved self-sensing of strain and damage has been shown in carbon fiber cement under flexure by three-point bending. This involves measurement of the one-dimensional distribution of the DC electrical resistance by the use of surface electrical contacts on the bottom (tension) and top (compression) surfaces. For a span of 290 mm, a spatial resolution of 5 mm has been attained. The bottom surface resistance, which increases reversibly with strain and increases irreversibly with damage, is a more effective indicator of strain and damage (in combination) than the top surface resistance, the oblique resistance or the through-thickness resistance for spatially resolved self-sensing. For sensing without spatial resolution, the oblique resistance is the most effective indicator. For sensing with distinction between strain and damage, the top surface resistance is the most effective indicator.

Introduction

Self-sensing refers to the ability of a structural material to sense itself (such as its damage and strain) without embedded or attached sensors. The advantages of self-sensing over the use of embedded or attached sensors are low cost, high durability, large sensing volume and absence of mechanical property loss. Applications include traffic monitoring, building monitoring, weighing, homeland security, structural vibration control, and structural health monitoring and hazard mitigation.

The self-sensing of strain [1–17] and damage [13–21] has been shown in cement containing discontinuous carbon fiber. This ability stems from the reversible change of the electrical resistivity with strain (a phenomenon known as piezoresistivity) and the irreversible change of the resistivity with damage. Although this ability has been shown under tension, compression and flexure, prior work has been limited to self-sensing without spatial resolution, i.e., self-sensing to obtain information on the overall specimen rather than information on various parts of a specimen. Spatially resolved sensing is practically important, due to the need to determine the location of damage or strain.

The effectiveness of spatially resolved sensing depends on the electrical resistivity of the material. A low resistivity will cause the current applied at a particular location in the specimen to spread, thus limiting the spatial resolution. Thus, a self-sensing material of high resistivity is desirable for providing spatial resolution.

The resistivity of carbon fiber cement decreases by orders of magnitude at the percolation threshold, which is the volume fraction above which the fibers contact one another and form a continuous conduction path [22]. For cement paste containing carbon fiber and silica fume, which is for enhancing the fiber dispersion, the percolation threshold is between 0.5 and 1.0 vol.% [22]. Most prior work on the self-sensing behavior of carbon fiber cement uses a fiber content of 0.5 vol.%, which is just below the percolation threshold. Percolation is not required for the self-sensing behavior. This work also uses a fiber content of 0.5 vol.%. Because of the low fiber content, the electrical resistivity of the cement-based material is quite high. The high value is favorable for spatially resolved self-sensing.

S. Wen · D. D. L. Chung (✉)
Composite Materials Research Laboratory, University at Buffalo
State University at New York, Buffalo, NY 14260-4400, USA
e-mail: ddlchung@buffalo.edu

This paper is aimed at investigating the ability of carbon fiber cement for spatially resolved self-sensing. For this purpose, non-uniform damage or strain needs to be imposed on a specimen. Flexural loading of a beam results in greatest stress at the middle of the span of the beam. In contrast, tensile or compressive loading tends to result in uniform stress along the whole length of the specimen (along the stress axis). Therefore, this work uses flexural loading.

Electrical resistance measurement is preferably conducted using the four-probe method rather than the two-probe method. This is because the four-probe method involves separate voltage and current probes (two outer probes for passing current and two inner probes for voltage measurement), whereas the two-probe method involves two probes, such that each probe serves for both current application and voltage measurement. Due to the separate voltage and current probes, the resistance obtained with the four-probe method excludes the resistance of the electrical contacts. In contrast, the resistance obtained with the two-probe method includes the resistance of the electrical contacts. This work uses the four-probe method, as in most previous work. However, 16 electrical contacts (8 on each of two surfaces) are involved for the same specimen in this work, in order to measure the electrical resistance of five (or more) segments of the specimen for the purpose of spatial distribution sensing.

Flexure involves tension on one side of the specimen and compression on the opposite side. Thus, this work uses separate electrical contacts on the tension surface and on the compression surface [1, 17], so that the surface resistance (as opposed to the volume resistance) of each surface is monitored during flexure. In addition, by using two contacts on the tension surface and two directly opposite contacts on the compression surface, this work measures the through-thickness resistance [17]. Furthermore, by using two contacts on the tension surface and two contacts that are not directly opposite on the compression surface, this work measures the oblique resistance [17]. The through-thickness direction is in the loading direction, perpendicular to the tension and compression surfaces. The oblique resistance is at an angle between the through-thickness direction and the plane of the tension or compression surface.

Experimental methods

Materials

The carbon fibers were isotropic pitch based and unsized, as obtained from Ashland Petroleum Co. (Ashland, KY). The fiber diameter was 15 μm. The nominal fiber length was 5 mm. Fibers in the amount of 0.50% by mass of cement (corresponding to 0.48 vol.%) were used. Prior to using the fibers in cement, they were dried at 110 °C in air for 1 h and then surface treated with ozone by exposure to O_3 gas (0.6 vol.%, in O_2) at 160 °C for 10 min. The ozone treatment was for improving the wettability of fibers by water [7].

The cement used was Portland cement (Type I) from Lafarge Corp. (Southfield, MI). The silica fume (Elkem Materials Inc., Pittsburgh, PA, microsilica, EMS 965) was used in the amount of 15% by mass of cement. The methylcellulose, used in the amount of 0.4% by mass of cement, was Dow Chemical Corp., Midland, MI, Methocel A15−LV. The defoamer (Colloids Inc., Marietta, GA, 1010) used whenever methylcellulose was used was in the amount of 0.13 vol.% (% of specimen volume).

A rotary mixer with a flat beater was used for mixing. Methylcellulose was dissolved in water and then the defoamer and fibers were added and stirred by hand for about 2 min. Then, the methylcellulose mixture, cement, water, and silica fume were mixed for 5 min. After pouring the mix into oiled molds, an external electric vibrator was used to facilitate compaction and decrease the amount of air bubbles. The specimens were demolded after 1 day and then allowed to cure at room temperature in air (relative humidity = 100%) for 28 days. The water/cement ratio was 0.35. Three specimens were tested for each type of resistance measurement (top surface, bottom surface, through-thickness and oblique resistances) in order to confirm the reproducibility of the results of this work.

Testing methods

The specimen was a rectangular bar of size 320 × 40 × 40 mm. Electrical contacts in the form of silver paint in conjunction with copper wire were applied on the tension and compression surfaces. Contacts A_1, A_2,... A_8 were on the compression (top) surface; contacts B_1, B_2,... B_8 were on the tension (bottom) surface, as illustrated in Fig. 1. Each contact was in the form of a strip in the transverse direction on the tension or compression surface. The various contact strips were parallel to one another.

The specimen configuration for flexural testing (three-point bending at a span of 290 mm) is illustrated in Fig. 1. With the span and electrical contacts fixed, the loading was successively directed at P, Q and R. Adjacent points P and Q were 5 mm apart; adjacent points Q and R were also 5 mm apart. The three points in set P are symmetrically positioned relative to the mid-point of the length of the specimen. Those in sets Q and R are asymmetrically positioned. The use of point sets P, Q, and R provides three stress distributions for demonstration of spatially resolved

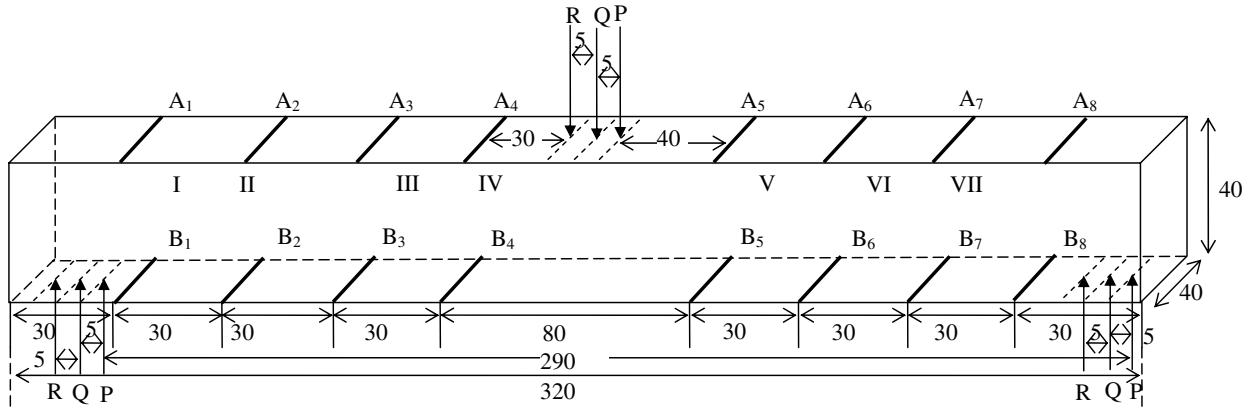

Fig. 1 Specimen configuration for flexural testing by three-point bending. The three points are shown by arrows. A_1, A_2, ... A_8 are electrical contacts on the compression (top) surface, whereas B_1, B_2,... B_8 are electrical contacts on the tension (bottom) surface. All dimensions are in mm. The segments are labeled I, II, III, IV, V, VI, and VII. Three sets (labeled P, Q, and R) of three points per set were separately used for the three-point bending. The three points in set P are symmetrically positioned relative to the mid-point of the length of the specimen. Those in sets Q and R are asymmetrically positioned. The span is 290 mm for each of the three sets. The specimen length is 320 mm. Points P and Q were 5 mm apart. Points Q and R are also 5 mm apart

sensing. For each of sets P, Q, and R, flexural loading at progressively increasing stress amplitude up to failure was imposed and three specimens were tested.

The compression (top) surface resistance was measured by using (i) A_1 and A_4 as current contacts and A_2 and A_3 as voltage contacts (for Segment II), (ii) A_2 and A_5 as current contacts and A_3 and A_4 as voltage contacts (for Segment III), (iii) A_3 and A_6 as current contacts and A_4 and A_5 as voltage contacts (for Segment IV), (iv) A_4 and A_7 as current contacts and A_5 and A_6 as voltage contacts (for Segment V), and (v) A_5 and A_8 as current contacts and A_6 and A_7 as voltage contacts (for Segment VI).

The tension (bottom) surface resistance was measured by using (i) B_1 and B_4 as current contacts and B_2 and B_3 as voltage contacts (for Segment II), (ii) B_2 and B_5 as current contacts and B_3 and B_4 as voltage contacts (for Segment III), (iii) B_3 and B_6 as current contacts and B_4 and B_5 as voltage contacts (for Segment IV), (iv) B_4 and B_7 as current contacts and B_5 and B_6 as voltage contacts (for Segment V), and (v) B_5 and B_8 as current contacts and B_6 and B_7 as voltage contacts (for Segment VI).

The through-thickness resistance was measured by using (i) A_1 and B_1 as current contacts and A_2 and B_2 as voltage contacts (for Segment I), (ii) A_2 and B_2 as current contacts and A_3 and B_3 as voltage contacts (for Segment II), (iii) A_3 and B_3 as current contacts and A_4 and B_4 as voltage contacts (for Segment III), (iv) A_4 and B_4 as current contacts and A_5 and B_5 as voltage contacts (for Segment IV), (v) A_5 and B_5 as current contacts and A_6 and B_6 as voltage contacts (for Segment V), (vi) A_6 and B_6 as current contacts and A_7 and B_7 as voltage contacts (for Segment VI), and (vii) A_7 and B_7 as current contacts and A_8 and B_8 as voltage contacts (for Segment VII).

The oblique resistance was measured by using (i) A_1 and B_4 as current contacts and A_2 and B_3 as voltage contacts (for Segment II), (ii) A_2 and B_5 as current contacts and A_3 and B_4 as voltage contacts (for Segment III), (iii) A_3 and B_6 as current contacts and A_4 and B_5 as voltage contacts (for Segment IV), (iv) A_4 and B_7 as current contacts and A_5 and B_6 as voltage contacts (for Segment V), and (v) A_5 and B_8 as current contacts and A_6 and B_7 as voltage contacts (for Segment VI).

Loading was provided by a hydraulic mechanical testing system (MTS 810), which also provided measurement of the displacement during flexure. During the testing, the resistances of the five (or more) segments were measured successively and continuously, such that the time between successive measurements was 0.3 s. A Keithley 2002 multimeter was used for DC resistance measurement using the four-probe method.

Results and discussion

Figure 2 shows the fractional change in resistance during flexural loading at point set P at progressively increasing deflection amplitudes up to failure for the surface resistance on the tension (bottom) side. This resistance increases upon loading. The reversible portion of the resistance increase is due to strain; the irreversible portion is due to damage. The higher is the deflection, the greater is the irreversible portion. At failure, the resistance increases abruptly. The trends are the same for the five segments (II, III, IV, V, and VI) shown in Fig. 2, but the fractional change in resistance at the same deflection is higher for Fig. 2(c) (Segment IV) than for Fig. 2(b) (Segment III) and

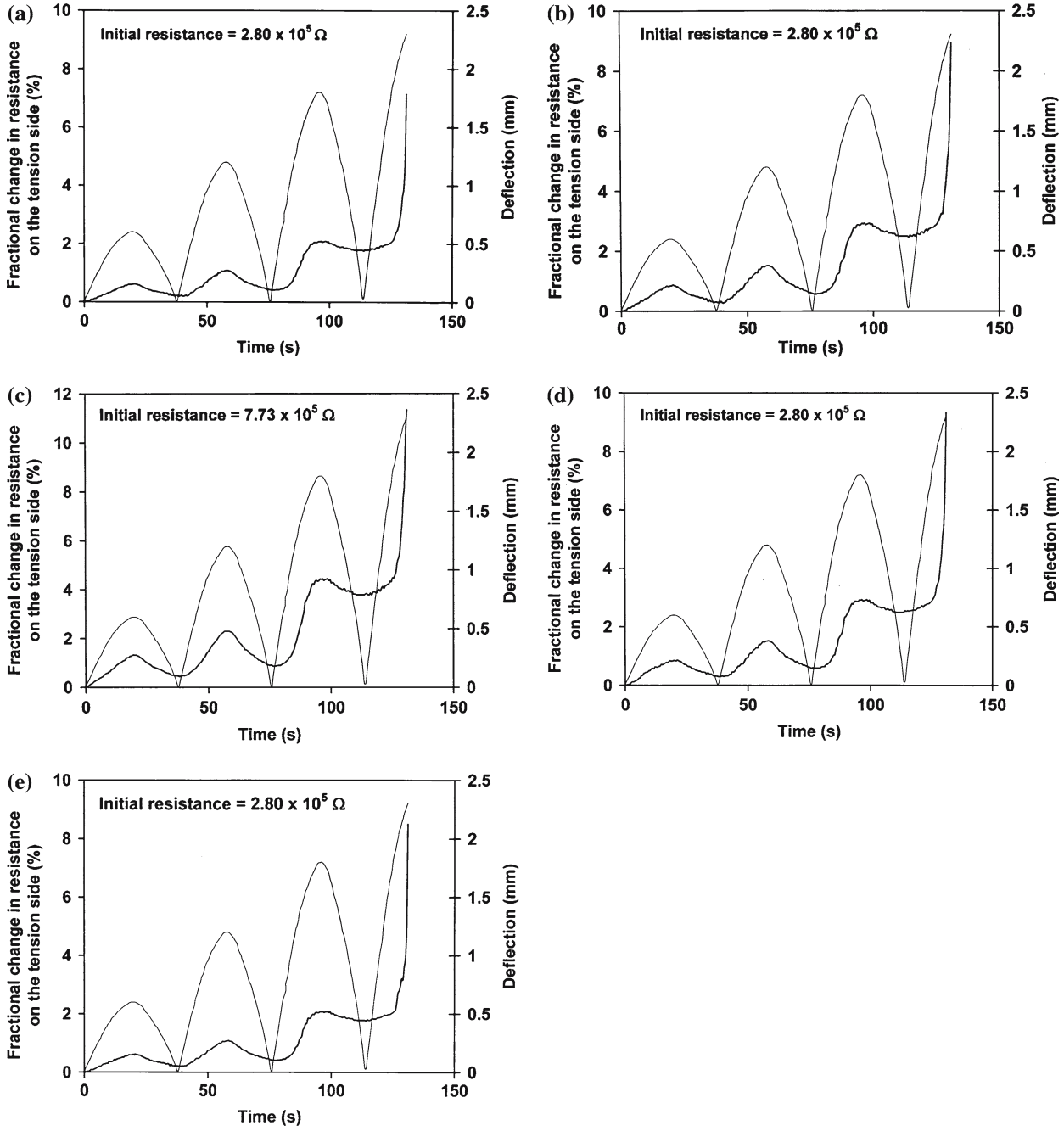

Fig. 2 Fractional change in resistance of the tension (bottom) surface (thick curve) and deflection (thin curve) during repeated flexure at point set P at progressively increasing stress amplitude up to failure. (a) Resistance between B_2 and B_3 (Segment II). (b) Resistance between B_3 and B_4 (Segment III). (c) Resistance between B_4 and B_5 (Segment IV). (d) Resistance between B_5 and B_6 (Segment V). (e) Resistance between B_6 and B_7 (Segment VI)

2(d) (Segment V), which are similar. The fractional change in resistance is in turn higher for Fig. 2(b) (Segment III) and 2(d) (Segment V) than Fig. 2(a) (Segment II) or 2(e) (Segment VI). Hence, the closer the segment is to the middle of the span, the greater is the fractional change in resistance at a given midspan deflection. This is because of the higher strain and damage associated with greater proximity to the midspan position. Thus, spatially resolved sensing is shown.

Figures 3, 4 5 show corresponding results for point set P for the oblique resistance, through-thickness resistance and top (compression) surface resistance respectively. The top (compression) surface resistance decreases in every cycle for every segment, as expected for compression. The

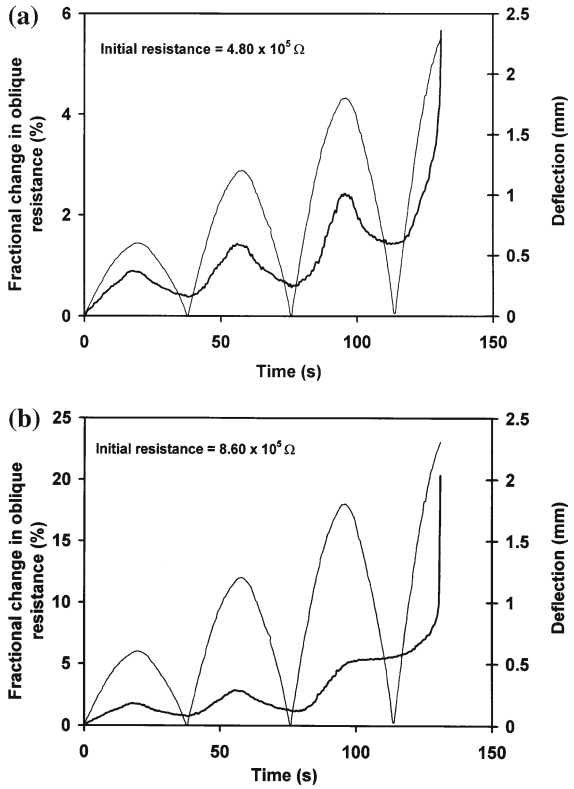

Fig. 3 Fractional change in resistance of the oblique (thick curve) and deflection (thin curve) during repeated flexure at point set P at progressively increasing stress amplitude up to failure. (a) Segment II. (b) Segment IV

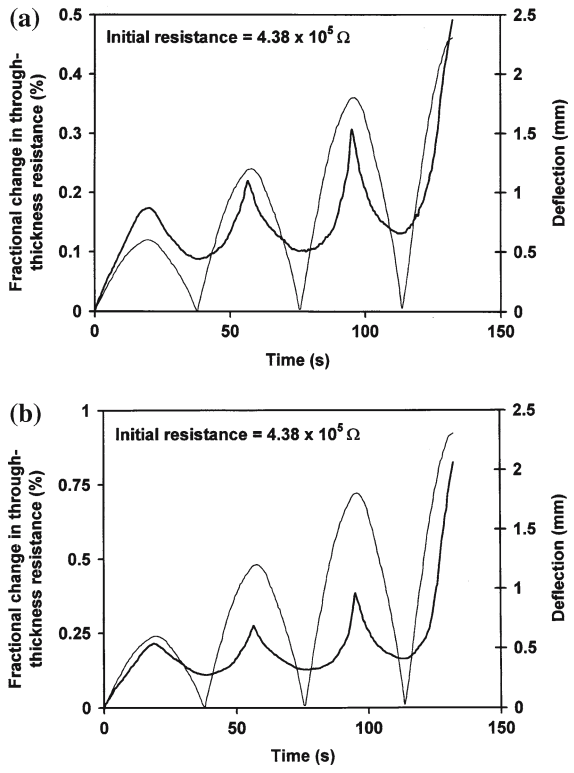

Fig. 4 Fractional change in resistance of the through-thickness (thick curve) and deflection (thin curve) during repeated flexure at point set P at progressively increasing stress amplitude up to failure. (a) Segment II. (b) Segment IV

oblique and through-thickness resistances increase in every cycle for every segment.

A quantitative description of the sensing ability is the ratio of the peak value of the fractional change in resistance to that of the midspan deflection for each cycle, as shown in Tables 1–3 (for loading at point sets P, Q, and R respectively) for each segment and for each type of resistance (top surface, bottom surface, oblique and through-thickness resistances). In relation to damage sensing, Cycle 3 is most relevant, as the resistance change in this cycle is dominated by damage rather than strain. Cycle 4 is less revealing, because failure occurs within this cycle.

For both the top surface and bottom surface resistances, the ratio (Tables 1–3) is highest in magnitude for the middle segment (Segment IV) for every cycle, since the middle segment encounters more strain than the other segments. For the oblique resistance, the ratio is highest for Segment III, followed closely by Segment IV, for every cycle. For the through-thickness resistance, the ratio is highest for Segment III (or Segments III and IV) for every cycle. Thus, the top and bottom surface resistances are more indicative of the strain distribution than the oblique or through-thickness resistance. Nevertheless, spatially resolved sensing has been attained for any of the four types of resistance.

For a given segment and a given resistance type (other than the through-thickness resistance), the ratio becomes more positive (or less negative) as the cycle number increases from 2 to 3 and then to 4. This is because of the increase in damage as the cycle number and its associated midspan deflection increase. Whether the strain causes the resistance to increase (as for the bottom surface and oblique resistances) or decrease (as for the top surface resistance), damage causes the resistance to increase.

Both damage and strain affect the peak resistance of a cycle, which the data in Tables 1–3 reflect. Distinction between damage and strain requires information on the reversibility of the resistance change, as shown in Figs. 2–5. The irreversible portion of a resistance change indicates damage, whereas the reversible portion indicates strain.

For a given segment and a given cycle, the magnitude of the resistance change, as shown by the magnitude of the ratio (Tables 1–3), is highest for the oblique resistance, followed by the bottom (tension) surface resistance. The superior sensitivity provided by the oblique resistance is attributed to the oblique direction of the current path,

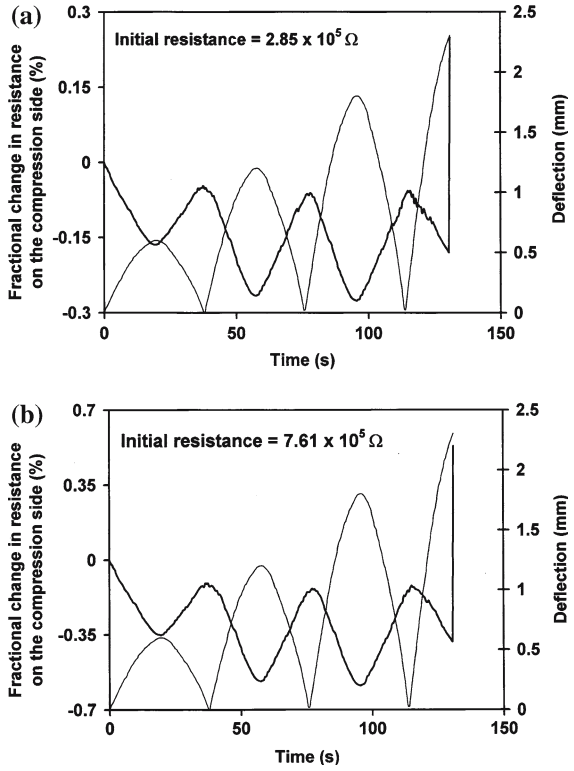

Fig. 5 Fractional change in resistance of the compression (top) surface (thick curve) and deflection (thin curve) during repeated flexure at point set P at progressively increasing stress amplitude up to failure. (a) Segment II (b) Segment IV

which allows probing of the entire thickness and length of the segment. In contrast, the surface resistances do not give information on the entire thickness and the through-thickness resistance does not give information on the entire segment.

Comparison among Tables 1–3 shows that the magnitude of the ratio increases progressively from Table 1 (for loading at point set P) to Table 2 (for loading at point set Q) and then to Table 3 (for loading at point set R) for any of Segments I, II and III, but decreases progressively from Table 1 to Table 2 and to Table 3 for any of Segments V, VI, and VII. These trends from one table to another uniformly apply to all of Cycles 1–4 and to all of the four resistance types listed in Tables 1–3. The trends are clear in spite of the substantial ± range for each entry in Tables 1–3. This means that the different strain/damage distributions associated with P, Q, and R can be distinguished by measuring the resistance in Segments I, II, III, V, VI or VII.

The increasing magnitude trend for Segments I, II, and III is due to the decreasing distance of each of these segments to the midspan position, which is the position of maximum deflection. For example, Segment III is closer to the midspan position for point set Q than that for point set P. Greater proximity to the midspan position causes more strain and damage in the segment and hence more change in resistance. In particular, greater proximity to the midspan position is expected to cause more damage in the segment and more damage results in the resistance becoming more positive (or less negative). The increasing magnitude trend (increasingly positive) from Table 1 to Table 2 and then to Table 3 for Cycle 4 and the top surface resistance is due to increasing damage, whereas the increasing magnitude trend

Table 1 Ratio of the peak value of the fractional change in resistance to that of the midspan deflection for each cycle of each segment

Resistance type	Segment No.	Ratio (10^{-4} mm^{-1})			
		Cycle 1	Cycle 2	Cycle 3	Cycle 4
Top (compression) surface	II	−8.51 ± 0.89	−5.26 ± 0.53	−3.16 ± 0.40	10.8 ± 1.5
	III	−13.5 ± 1.04	−7.69 ± 0.91	−5.50 ± 0.67	15.1 ± 1.8
	IV	−20.5 ± 2.30	−12.2 ± 1.40	−7.66 ± 0.92	23.0 ± 3.2
	V	−14.5 ± 1.8	−8.19 ± 0.75	−5.33 ± 0.63	15.6 ± 1.7
	VI	−8.35 ± 1.01	−5.01 ± 0.62	−3.28 ± 0.45	10.4 ± 1.4
Bottom (tension) surface	II	102 ± 10	87 ± 10	116 ± 16	310 ± 45
	III	146 ± 15	125 ± 14	161 ± 20	388 ± 50
	IV	214 ± 18	191 ± 23	247 ± 31	492 ± 58
	V	139 ± 16	125 ± 15	160 ± 14	405 ± 43
	VI	100 ± 12	91 ± 11	112 ± 13	369 ± 41
Oblique	II	145 ± 13	117 ± 13	132 ± 15	245 ± 33
	III	340 ± 40	268 ± 28	338 ± 39	1062 ± 120
	IV	291 ± 33	233 ± 22	290 ± 34	883 ± 100
	V	189 ± 21	151 ± 17	132 ± 11	460 ± 56
	VI	124 ± 10	100 ± 13	110 ± 10	198 ± 27
Through-thickness	I	19.7 ± 2.4	12.6 ± 1.1	11.4 ± 1.3	14.9 ± 1.8
	II	29.0 ± 3.7	18.0 ± 1.9	16.6 ± 2.4	21.3 ± 2.4
	III	35.4 ± 3.4	23.0 ± 3.0	21.7 ± 2.6	35.3 ± 4.0
	IV	35.1 ± 4.2	22.3 ± 2.7	21.9 ± 2.6	35.7 ± 3.9
	V	29.4 ± 3.1	17.5 ± 2.2	16.7 ± 1.5	20.8 ± 2.3
	VI	19.2 ± 2.4	12.5 ± 1.5	11.6 ± 1.0	15.2 ± 1.7
	VII	10.6 ± 1.4	6.7 ± 0.8	6.4 ± 0.8	8.2 ± 0.9

The loading was at point set P (Fig. 1)

Table 2 Ratio of the peak value of the fractional change in resistance to that of the midspan deflection for each cycle of each segment

Resistance type	Segment No.	Ratio (10^{-4} mm^{-1})			
		Cycle 1	Cycle 2	Cycle 3	Cycle 4
Top (compression) surface	II	−8.55 ± 0.80	−5.34 ± 0.57	−3.22 ± 0.38	11.1 ± 1.6
	III	−13.8 ± 1.10	−7.81 ± 1.04	−5.62 ± 0.60	15.7 ± 1.8
	IV	−21.6 ± 2.7	−12.0 ± 1.50	−7.83 ± 0.90	23.7 ± 3.1
	V	−14.1 ± 1.6	−8.05 ± 0.82	−5.16 ± 0.71	15.1 ± 1.6
	VI	−8.20 ± 0.94	−4.92 ± 0.70	−3.22 ± 0.40	10.1 ± 1.5
Bottom (tension) surface	II	103 ± 12	89 ± 10	119 ± 15	320 ± 47
	III	150 ± 17	128 ± 13	164 ± 19	401 ± 50
	IV	217 ± 23	186 ± 21	241 ± 33	506 ± 56
	V	133 ± 15	122 ± 16	155 ± 17	398 ± 41
	VI	98 ± 13	89 ± 10	110 ± 12	362 ± 45
Oblique	II	151 ± 17	122 ± 16	135 ± 14	253 ± 32
	III	346 ± 43	274 ± 30	350 ± 44	1102 ± 140
	IV	297 ± 35	241 ± 26	308 ± 33	914 ± 130
	V	183 ± 20	144 ± 16	122 ± 13	438 ± 67
	VI	121 ± 14	98 ± 13	107 ± 14	192 ± 29
Through-thickness	I	20.0 ± 2.6	12.9 ± 1.3	11.5 ± 1.2	15.2 ± 1.7
	II	29.5 ± 3.5	18.4 ± 2.1	17.0 ± 1.9	21.8 ± 2.6
	III	35.9 ± 3.7	23.5 ± 2.9	22.3 ± 2.8	36.1 ± 4.5
	IV	34.6 ± 4.0	22.0 ± 2.5	20.5 ± 2.7	35.1 ± 4.2
	V	29.1 ± 3.2	17.2 ± 2.4	16.2 ± 1.5	20.3 ± 2.5
	VI	19.4 ± 2.3	12.3 ± 1.4	11.2 ± 1.2	15.6 ± 1.9
	VII	10.5 ± 1.3	6.6 ± 0.9	6.4 ± 0.8	8.1 ± 1.0

The loading was at point set Q (Fig. 1)

Table 3 Ratio of the peak value of the fractional change in resistance to that of the midspan deflection for each cycle of each segment

Resistance type	Segment No.	Ratio (10^{-4} mm^{-1})			
		Cycle 1	Cycle 2	Cycle 3	Cycle 4
Top (compression) surface	II	−9.02 ± 1.20	−6.00 ± 0.73	−3.55 ± 0.42	12.6 ± 1.8
	III	−14.8 ± 1.50	−8.98 ± 1.24	−6.49 ± 0.80	18.1 ± 2.3
	IV	−24.1 ± 2.6	−13.7 ± 1.60	−8.95 ± 1.10	27.4 ± 3.4
	V	−13.1 ± 1.5	−7.17 ± 0.93	−4.03 ± 0.61	13.5 ± 1.7
	VI	−7.60 ± 0.90	−4.23 ± 0.60	−2.44 ± 0.35	8.9 ± 1.2
Bottom (tension) surface	II	110 ± 13	103 ± 11	130 ± 16	347 ± 48
	III	161 ± 19	144 ± 16	186 ± 21	440 ± 58
	IV	240 ± 25	208 ± 24	278 ± 34	590 ± 63
	V	120 ± 15	105 ± 14	130 ± 16	350 ± 41
	VI	91 ± 12	82 ± 10	102 ± 14	343 ± 49
Oblique	II	160 ± 19	131 ± 14	156 ± 18	264 ± 32
	III	372 ± 42	303 ± 34	397 ± 46	1240 ± 150
	IV	314 ± 37	259 ± 30	340 ± 35	1026 ± 140
	V	170 ± 22	128 ± 17	97 ± 14	446 ± 68
	VI	113 ± 16	88 ± 12	92 ± 14	173 ± 26
Through-thickness	I	20.9 ± 2.5	13.8 ± 1.6	12.3 ± 1.5	15.8 ± 1.9
	II	31.7 ± 3.3	19.2 ± 2.2	18.5 ± 2.1	23.4 ± 2.8
	III	40.6 ± 4.4	26.8 ± 2.9	25.7 ± 3.1	41.8 ± 4.5
	IV	31.2 ± 3.6	20.1 ± 2.4	18.0 ± 2.4	33.3 ± 4.1
	V	27.5 ± 3.4	16.1 ± 1.9	14.9 ± 1.7	17.9 ± 2.3
	VI	18.6 ± 2.3	11.2 ± 1.5	10.0 ± 1.4	14.2 ± 2.0
	VII	9.8 ± 1.2	6.5 ± 0.9	6.0 ± 0.8	7.2 ± 0.9

The loading was at point set R (Fig. 1)

(increasingly negative) for Cycles 1–3 and the top surface resistance is due to increasing strain. On the other hand, the increasing magnitude trend (increasingly positive) from Table 1 to Table 2 and then to Table 3 for Cycles 1–4 and the bottom surface resistance and the oblique resistance is due to a combination of increasing strain and increasing damage, as both cause the resistance to become more positive. Thus, the top surface resistance is better for distinguishing between strain and damage than the other three types of resistance.

The decreasing magnitude trend for Segments V, VI, and VII is due to the increasing distance of each of these segments to the midspan position. For example, Segment V is farther from the midspan position for point set Q than that for point set P. Less proximity to the midspan position causes less strain and less damage and hence less change in resistance. The decreasing magnitude trend (decreasingly positive) from Table 1 to Table 2 and to Table 3 for Cycle 4 and the top surface resistance is due to decreasing damage, as decreasing strain would have caused the resistance change to be less negative (i.e., more positive – opposite to the observation). The decreasing magnitude trend (decreasingly negative) from Table 1 to Table 2 and to Table 3 for Cycles 1–4 and the top surface resistance is due to decreasing strain, as decreasing damage would have caused the resistance change to be less positive (i.e., more negative – opposite to the observation). On the other hand, the decreasing magnitude trend (decreasingly positive) from Table 1 to Table 2 and then to Table 3 for Cycles 1–4 and the bottom surface resistance and the oblique resistance is due to a combination of decreasing strain and decreasing damage, as both cause the resistance to become less positive.

The behavior is not as uniform for Segment IV, which contains the midspan position. This segment exhibits an increasing magnitude trend for most of the cases under the top and bottom surface resistances and for the oblique resistance, but exhibits a decreasing magnitude trend for the through-thickness resistance. This non-uniform behavior reflects (i) the complex changes in strain and damage distributions within Segment IV as loading moves from P to Q and then to R and (ii) the ineffectiveness of the overall resistance of Segment IV (which is longer than the other segments and contains points P, Q and R at the top surface) in distinguishing among the three different strain/damage distributions within Segment IV.

For a given combination of Segment No. and Cycle No., the change in the ratio from Table 2 to Table 3 is more than the corresponding change from Table 1 to Table 2. Since points P and Q are 5 mm apart and points Q and R are also 5 mm apart, the differences in data among Tables 1–3 show that a spatial resolution of 5 mm has been attained in the self-sensing. Since the change in the ratio from Table 1 to Table 2 is small, the limit of the spatial resolution is close to (or slightly better than) 5 mm.

For sensing strain and damage in combination, the bottom (tension) surface resistance and the oblique resistance are more effective indicators than the top (compression) surface resistance or the through-thickness resistance. This is due to the large effects of strain and damage on the bottom surface resistance and the oblique resistance. Without consideration of the spatial resolution, the oblique resistance is even more effective for sensing strain and damage in combination than the bottom (tension) surface resistance. This is because of the ability of the oblique resistance to indicate the condition of the interior region. In contrast, the surface resistance only indicates the condition of the surface region. However, if spatial resolution is important, the bottom surface resistance is a better indicator than the oblique resistance. This is due to the fact that the current and voltage contacts are not in line in the measurement of the oblique resistance. The sensing effectiveness is shown by the magnitude of the ratio of the peak value of the fractional change in resistance (relative to the resistance prior to loading) in a cycle to the midspan deflection in the cycle. This ratio provides a description of the extent of electrical resistance response to damage and strain in combination.

The spatial resolution is superior for the bottom (tension) surface resistance than the oblique resistance, as shown by the extent of bottom surface resistance response being maximum at midspan (as expected), and the extent of oblique resistance response being maximum at a distance of 30 mm from midspan. The lower spatial resolution of the oblique resistance compared to the bottom (tension) surface resistance is consistent with the fact that the current and potential gradient directions are not exactly the same in the measurement of the oblique resistance, whereas these directions are exactly the same in the measurement of the surface resistance.

The overall spatially resolved self-sensing performance is such that the bottom (tension) surface resistance is the best indicator. This resistance is also attractive due to the lower tendency for abuse of electrical contacts that are at the bottom surface (rather than the top surface) of a self-sensing concrete slab.

For sensing strain and damage such that strain and damage can be distinguished, the top (compression) surface resistance is the most effective indicator. The ratio is more positive when there is more damage, and is more negative when there is more strain. However, the effects of strain and damage on this resistance is relatively small.

This work is limited to spatial resolution in one dimension. Spatial resolution in two dimensions is needed in numerous applications. Nevertheless, the results of this work on one-dimensional spatial resolution provides the basis for extension to two dimensions.

This work provides the first demonstration of spatially resolved self-sensing in cement-based materials. This demonstration uses flexural loading to provide a stress distribution along the axis of the span. A related scenario involves the application of impact at a point along the length of a specimen bar, but this scenario pertains to damage sensing without strain sensing. The sensing of impact on carbon fiber cement is the subject of another paper.

Conclusion

Spatially resolved self-sensing of strain and damage has been demonstrated in carbon fiber cement under flexure by three-point bending with a span of 290 mm. By measuring the DC electrical resistance of different 30-mm long segments of the specimen for each of three stress distributions that are displaced relative to one another by 5 mm, a one-dimensional spatial resolution of 5 mm has been shown. The resistance measurement involves the use of electrical contacts on the top (compression) and bottom (tension) surfaces. The use of four electrical contacts at a time allows measurement of the resistance of each segment. The resistance of each segment can be the bottom (tension) surface resistance, the top (compression) surface resistance, the oblique resistance or the through-thickness resistance. The bottom surface resistance is the best indicator for spatially resolved self-sensing of strain and damage in combination, due to the large effects of strain and damage on this resistance. For self-sensing without spatial resolution, the oblique resistance is the best indicator, due to its ability to sense the interior region. For self-sensing with distinction between strain and damage, the top surface resistance is the best indicator, in spite of the small effects of strain and damage on this resistance.

Acknowledgement This work was supported in part by U.S. National Science Foundation.

References

1. Chen P-W, Chung DDL (1996) Compos Part B-Eng 27B:11
2. Chung DDL (2002) J Intel Mat Syst Str 13(9):599
3. Wen S, Chung DDL (2003) Adv Cem Res 15(3):119
4. Chung DDL (2002) J Mater Eng Perform 11(2):194
5. Wen S, Chung DDL (2001) Cem Concr Res 31(2):297
6. Wen S, Chung DDL (2000) Cem Concr Res 30(8):1289
7. Fu X, Lu W, Chung DDL (1998) Carbon 36(9):1337
8. Fu X, Chung DDL (1997) Cem Concr Res 27(9):1313
9. Chen P-W, Chung DDL (1993) Smart Mater Struct 2:22
10. Wen S, Chung DDL (2001) Cem Concr Res 31(4):665
11. Wen S, Chung DDL (2005) ACI Mater J 102(4):244
12. Sun M, Mao Q, Li Z (1998) J Wuhan Univ Technol Mater Sci Ed. 13(3):58
13. Mao Q, Zhao B, Sheng D, Li Z (1996) J Wuhan Univ Technol 11(3):41
14. Reza F, Batson GB, Yamamuro JA, Lee JS (2003) J Mater Civil Eng 15(5):476
15. Wu Y, Bing C, Keru W (2003) Mech Mater Eng Sci Exp 172
16. Yao W, Chen B, Wu K (2003) J Mater Sci Technol 19(3):239
17. Wen S, Chung DDL J Mater Civil Eng, in press
18. Bontea D-M, Chung DDL, Lee GC (2000) Cem Concr Res 30(4):651
19. Fu X, Chung DDL (1996) Cem Concr Res 26(1):15
20. Chung DDL (2003) Mat Sci Eng R 42(1):1
21. Wen S, Chung DDL Carbon, in press
22. Chen P-W, Chung DDL (1995) J Electron Mater 24(1):47